CN^- molecular ions in silver halides: optical properties of a new isoelectronic exciton trap

1993 J. Phys.: Condens. Matter 5 7239

(http://iopscience.iop.org/0953-8984/5/39/011)

J. Phys.: Condens. Matter 5 (1993) 7239–7250. Printed in the UK

CN^- molecular ions in silver halides: optical properties of a new isoelectronic exciton trap

D Samiec, H Stolz and W von der Osten
Fachbereich Physik, Universität-GH, D-4790 Paderborn, Federal Republic of Germany

Received 1 March 1993, in final form 21 June 1993

Abstract. Low-temperature optical absorption and luminescence spectra of AgCl and AgBr doped with CN^- molecular defects are investigated. While in AgBr an amalgamation type of exciton is formed, CN^- in AgCl is found to act as an isoelectronic trap, producing a bound exciton state with a localization energy of about 350 meV. Evidence for strong lattice relaxation to stabilize this state is provided by the positions and lineshapes of the spectra. An exciton model is discussed to account for the strong temperature dependence of the decay time and intensities. The results are compared with those for atomic-type isoelectronic impurities in AgCl, like Br^- and I^-.

1. Introduction

In the silver halides AgCl and AgBr, isoelectronic impurities substitutionally built into the anion sublattices are known to act as efficient binding centres for excitons. The basic mechanism that produces a bound state originates from the difference in electron affinities between the host and the guest ions. In the (negative) impurity ion, the attached electron is less strongly bound than the one attached to the host ion. Therefore, at least at sufficiently low temperatures, the impurity can bind a hole. It becomes neutral in the ionic matrix and thus it can attract an electron forming a bound exciton (BX) state. The most thoroughly studied system of this type is AgBr:I^- for which a bound state exists with localization energy $E_l = 43$ meV (for references see Kanzaki 1986, von der Osten and Stolz 1990). It gives rise to characteristic luminescence which is strong enough to be observable even in the purest AgBr material, which always contains small concentrations of inadvertently present iodide.

In AgCl, bound exciton states are introduced and were investigated for doping with either bromide or iodide impurities (Joesten and Brown 1966, Ahrenkiel 1968). The main difference of these systems compared to AgBr:I^- lies in the increased electron (hole)–lattice interaction in this material that leads to additional stabilization and, as a consequence, to larger localization energies ($E_l = 337$ meV for AgCl:I^-; $E_l = 185$ meV for AgCl:Br^- (von der Osten and Stolz 1990)).

We recently started an investigation of molecular-type isoelectronic impurities doped into silver halides and in this paper report first results for CN^- molecular ions in both AgCl and AgBr. We measured and analysed the absorption and luminescence spectra of this impurity which in AgCl essentially behaves like an atomic isoelectronic centre, but in AgBr does not result in a bound state. In particular, the molecular character of the impurity apparently is not important, except with regard to the defect symmetry. Compared with hitherto investigated atomic-type isoelectronic centres, CN^- leads to a similar localization energy ($E_l \approx 350$ meV). The corresponding exciton luminescence exhibits a pronounced temperature dependence of decay time and intensity, the origin of which is discussed.

0953-8984/93/397239+12$07.50

2. Experimental results

2.1. Optical absorption

Because of the large spread in CN^- electron affinity values published in the literature (2.75 eV (Shriver and Posner 1966), 3.70 eV (Griffing and Simons 1976)) no predictions on the existence of a bound exciton state in AgCl:CN^- and AgBr:CN^- were possible (electron affinities 3.61 eV for Cl^-, 3.36 eV for Br^- (Hotop and Lineberger 1975)). For a systematic study we therefore prepared CN^- doped silver halide crystals with different CN^- doping levels. The crystals were grown by a standard Bridgman technique starting with powdered AgBr or AgCl and AgCN. After growth, the doping was checked by measuring the absorption strength of the CN^- stretching vibration in the infrared spectral region around 2072 cm^{-1}. With this no absolute values could be determined for the CN^- doping levels but the absorption strength was found to be proportional to the nominal CN^- concentrations of 10^{-5} to 10^{-2} mole fraction in the melt which are indicated in this paper.

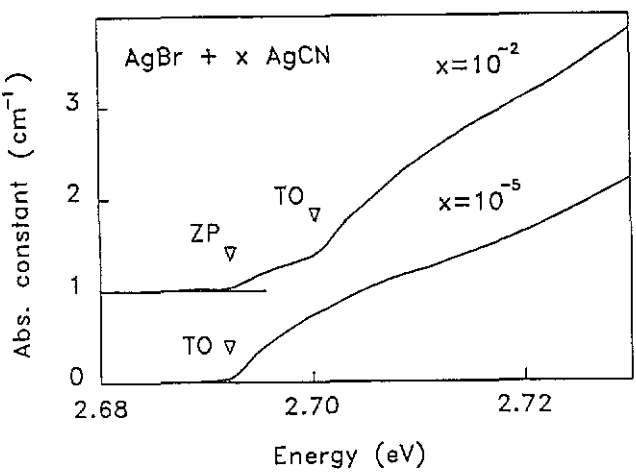

Figure 1. Absorption spectra of AgBr:CN^- for two CN^- concentrations near the indirect exciton edge at 20 K. The spectra are shifted along the ordinate. The energy positions of the zero-phonon (ZP) and TO(L) phonon-assisted components are marked. Spectral bandwidth: 0.2 meV.

In a first step we then investigated the absorption of the crystals close to the indirect free exciton (FE) absorption edge. As illustrated in figure 1, the effect of CN^- doping in AgBr consists in a high-energy shift of the absorption edge accompanied, at sufficiently large dopant levels, by the occurrence of a zero-phonon absorption component due to the relaxation of the k selection rule. This behaviour indicates that a BX state is not being formed, but rather an amalgamation type of exciton behaviour occurs.

Markedly different from this, in AgCl addition of CN^- gives rise to a broad absorption extending from the FE absorption edge ($E_{ax}^{i} = 3.256$ eV) to lower energies and growing in strength approximately proportional to the impurity concentration. In figure 2 we display this spectrum, together with the analogous Br^- induced absorption and a spectrum of nominally undoped AgCl (Stolz *et al* 1984). Comparing the integrated absorption between the two impurity-induced spectra, the oscillator strength in the case of CN^- is smaller by a factor of three, suggesting an exciton larger in spatial extension and, hence, with smaller overlap

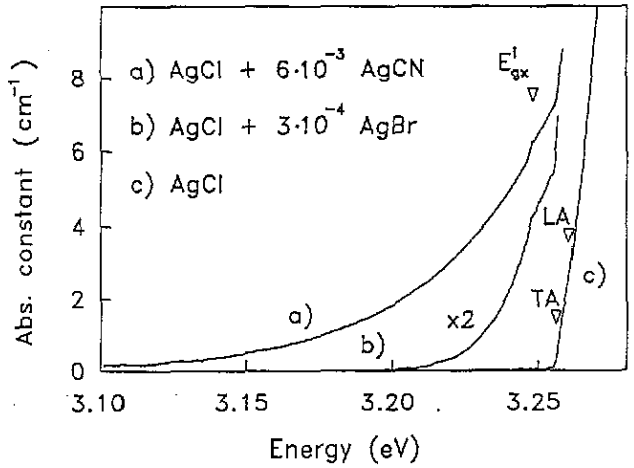

Figure 2. Absorption spectra of (*a*) AgCl:CN^- and (*b*) AgCl:Br^- in comparison with nominally pure AgCl (*c*) at 20 K. E^i_{gx}, TA and LA denote the energy positions of the indirect free exciton gap, the TA(L) and LA(L) phonon-assisted absorption components, respectively. Spectral bandwidth: 0.3 meV.

of the electron and hole wavefunctions (Joesten and Brown 1966). As for AgCl:Br^-, the lineshape of the CN^- induced low-energy absorption tail over three orders of magnitude follows an Urbach law nicely (see e.g. Toyozawa 1986)

$$\alpha(E, T) \sim \exp\left(-\sigma \frac{E_0' - E}{kT}\right) \tag{1}$$

where E_0' is the convergence point and σ is the steepness coefficient. A dependence on energy like this is anticipated for an exciton state with strong lattice relaxation around the defect. Since the ratio of steepness coefficients of Br^- and CN^- induced excitons deduced from fitting the experimental data in figure 2 amounts to $\sigma(CN^-)/\sigma(Br^-) = 0.28$, we suppose a larger exciton–phonon coupling strength for the CN^- compared with the Br^- induced exciton (Toyozawa 1986).

2.2. CN^- bound exciton luminescence

2.2.1. Spectra. The difference between the absorption spectra of AgCl:CN^- and AgBr:CN^- is also reflected in the luminescence properties. In AgBr, excitation slightly above the exciton absorption edge essentially causes, besides the iodine BX emission, the well-known broad donor–acceptor band to appear with a maximum around 2.2 eV (cf, e.g., Burberry and Marchetti 1985).

In contrast, the luminescence spectrum of AgCl:CN^- exhibits a strong dependence on excitation photon energy. Under excitation resonant with the CN^- absorption tail accomplished by a mercury lamp centred around 3.215 eV (spectral width: $\approx$ 25 meV), a new luminescence band is found (figure 3, upper) with its centre of gravity at 2.15 eV and of width 0.35 eV (FWHM). This band is clearly related to the CN^- impurity and on the basis of all properties, in particular its exponential time behaviour (see below), is ascribed to recombination of CN^- bound excitons.

Exciting the sample at 3.267 eV slightly above the exciton absorption edge, an additional weak band grows up with centre of gravity at 2.53 eV (figure 3, next lower spectrum). This

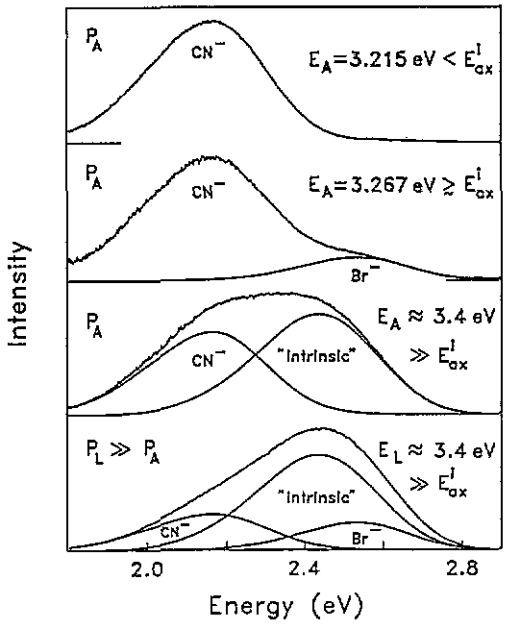

Figure 3. Luminescence spectra of AgCl + 10^{-3} AgCN under different excitation conditions: E_A, E_L denote the excitation photon energies of the mercury lamp and the laser, respectively. $P_A \approx 1$ mW and $P_L \approx 100$ mW are the corresponding excitation intensities. E^I_{ax} refers to the indirect absorption edge. The measured spectra are decomposed into various components as described in the text. $T = 20$ K except for the last spectrum measured at $T = 6$ K. Spectral bandwidth: 1 meV.

band has been previously observed and is attributed to excitons bound to bromine, which is present in small concentrations even in nominally undoped AgCl (Stolz *et al* 1984, Schulz and von der Osten 1993). Going to excitations still higher in the band (3.4 eV), the CN^- and Br^- induced exciton bands become superimposed with a broad luminescence band at 2.41 eV (figure 3, second from bottom) which is of intrinsic origin (Schulz and von der Osten 1993). At increasing power, when the impurities saturate, the spectrum depends strongly on excitation power with the intrinsic recombination dominating at high excitation intensities (figure 3, bottom).

In all cases the total luminescence intensity could unambiguously be decomposed into three luminescence components, namely the Br^-, CN^- and the intrinsic bands, as displayed in figure 3. At a given photon energy E_j we thus write

$$I_{tot}(E_j) = a_1 I_{Br}(E_j) + a_2 I_{CN}(E_j) + a_3 I_{intr}(E_j) \tag{2}$$

whereby peak positions and halfwidths of the separated Br^- and intrinsic components were taken from previous work (Schulz and von der Osten 1993). The CN^- component was deduced from our own resonant excitation measurements. By minimizing the mean square error it is straightforward to determine the coefficients a_1, a_2, and a_3 representing the relative strengths of the respective components.

To analyse the spectroscopic data of the BX(CN^-) we use the configurational coordinate diagram in figure 4 assuming linear exciton–phonon coupling (see e.g. Fitchen 1968). Because of the strong exciton–lattice interaction, a zero-phonon line (ZP) for the CN^- BX could not be detected. However, careful consideration of the absorption and luminescence bands at their low- and high-energy ends, respectively, suggests its position to be situated at $E_{ZP} = 2.90 \pm 0.10$ eV. This value, together with the energy position of the luminescence maximum (E_{max} in figure 4), enables us to derive various energies that characterize the exciton (cf caption of figure 4). From the ZP line relative to the indirect FE gap energy ($E^i_{gx} = 3.248$ eV), the localization energy of the BX state is $E_l = (0.35 \pm 0.10)$ eV. The

lattice relaxation energy E_{LR} and the bare electronic energy E_0 can also be determined and are found to be $E_{LR} = (0.75 \pm 0.10)$ eV and $E_0 = (3.65 \pm 0.10)$ eV, respectively. These quantities are listed in table 1.

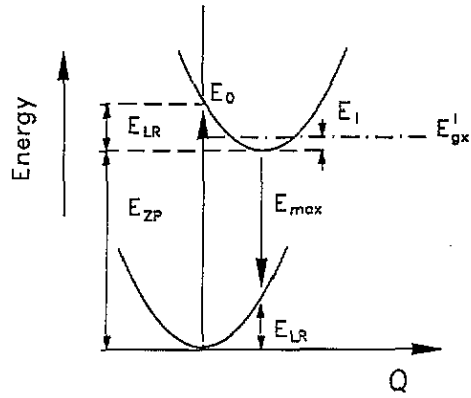

Figure 4. Configuration coordinate diagram defining the energies used in the analysis (see text). The following relations between the energies hold: $E_{LR} = E_{ZP} - E_{max}$, $E_0 = 2E_{LR} - E_{max}$, $E_1 = E^i_{gx} - E_{ZP}$.

Table 1. Relevant energies (in eV) of excitons bound to isoelectronic impurities in AgCl. For definitions see figure 4. ΔE_a are the differences in electron affinities (3.61, 3.36 and 3.06 eV for Cl^-, Br^- and I^- (Hotop and Lineberger 1975); values between 3.36 and 3.61 eV were chosen for CN^- (see text)).

Defect	ΔE_a	$E_0 - E^i_{gx}$	E_1	E_{LR}
AgCl:CN^-	0...0.25	0.40 ± 0.10	0.35 ± 0.10	0.75 ± 0.10
AgCl:Br^-	0.25	0.35	0.185	0.53
AgCl:I^-	0.55	−0.10	0.337	0.23

2.2.2. Temperature dependence of intensity. To further explore the nature of the CN^- BX band, we investigated the integrated luminescence intensity as a function of temperature. In these measurements excitation was accomplished at 3.4 eV (see bottom spectrum in figure 3), and the various contributions to the total luminescence intensity were obtained by the analysis described above. As displayed in the log intensity against $1/T$ plot in figure 5, the strength of the CN^- BX band at very low temperatures remains constant up to about 20 K and is then strongly reduced, becoming smaller by three orders of magnitude at about 30 K. Assuming thermal activation as the origin of the reduction, the temperature-dependent intensity $I(T)$ can be written as

$$I(T)/I(0) = 1 + g^* \exp(-\Delta E_{act}/kT) \tag{3}$$

where $g*$ is the ratio of degeneracies and transition probabilities of the involved states. Fitting the experimental data, an activation energy $\Delta E_{act} = (18 \pm 5)$ meV is derived. This value is close to the binding energy of the FE in AgCl ($E^i_{bx} \approx 23$ to 40 meV (see e.g.

von der Osten 1982, 1984), but much less than the localization energy of the CN^- BX ($E_l \approx 350$ meV, see above). This implies that the dominant quenching process is thermal ionization of the exciton (leaving behind the hole bound to the impurity) rather than the formation of a FE plus the remaining CN^- impurity. A completely analogous behaviour is found for the Br^- induced exciton luminescence also shown in figure 5. The smaller intensity here, however, does not allow us to determine the activation energy accurately.

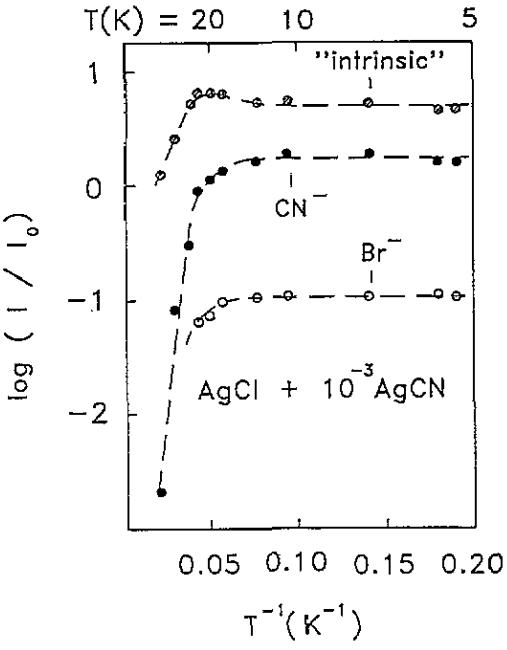

Figure 5. Integrated intensities of the CN^- and Br^- BX luminescence components plotted against inverse sample temperature in AgCl + 10^{-3} AgCN. The Br^- BX luminescence originates from unintentionally present impurities. Also shown is the intensity of the intrinsic luminescence.

2.2.3. Temporal behaviour. To reveal finer details of the electronic structure of the exciton measurements of the time decay of the luminescence after chopped excitation were essential. These were performed by means of a boxcar system. Otherwise we again used the spectral excitation conditions that led to the spectrum in figure 3 (bottom). Consistent with the superposition of various luminescence components, we found the time behaviour to depend on the detection photon energy E_D. Two typical cases are illustrated in figure 6. For $E_D = 2.43$ eV the intensity mainly stems from the intrinsic luminescence band, giving rise to non-exponential decay as expected. Monitoring the emission at lower energy ($E_D = 2.00$ eV), the CN^- BX luminescence prevails and causes initial exponential components in the decay curve, characterized by two time constants τ_A and τ_B, implying a splitting of the CN^- BX state into two substates. In analysing these data, we actually found that the total time-dependent intensity in this spectral region can be represented by

$$I_{tot}(E_D, t) = \sum_{i=A,B} a_i(E_D) \exp(-t/\tau_i) + \sum_{j=0}^{\infty} a_j(E_D) \exp(-t/\tau_j). \tag{4}$$

The first term on the right-hand side accounts for the CN^- BX decay and the second term models the non-exponential decay of the intrinsic luminescence, each with amplitudes depending on E_D. Because of the difference between the chopping times of the excitation

and the luminescence lifetimes, the measured amplitudes may deviate from the real ones and have to be corrected (Samiec 1990). Performing this correction, the amplitude ratio derived from the decay curves at zero time nicely agreed with those deduced from decomposing the total spectrum (figure 3). It demonstrates the consistency of our analysis and implies that the two exponentially decaying luminescence components A and B are related to the CN^- BX state.

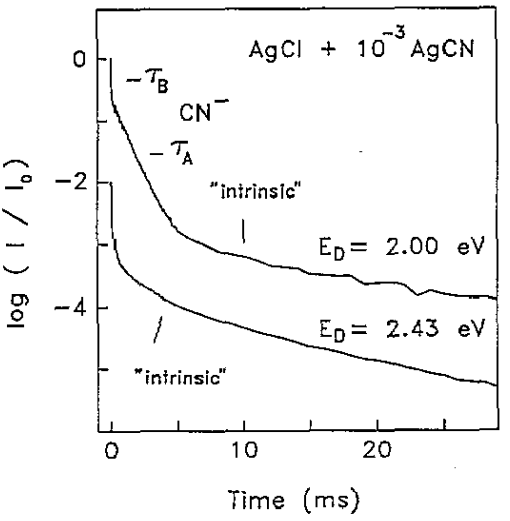

Figure 6. Decay of the total luminescence intensity of AgCl + 10^{-3} AgCN at two detection photon energies E_D. Laser excitation at E_L = 3.4 eV. T = 6 K. The fast decay with time constants τ_A, τ_B is due to the CN^- bound exciton, the non-exponential decay to the intrinsic luminescence.

Another important result is the surprisingly strong variation of the luminescence decay with temperature, displayed in figure 7. To obtain these data, the non-exponential decay due to the intrinsic luminescence (at the respective temperatures) was subtracted. Within the temperature range 1.8 to 13 K the CN^- BX component B decays with time constant $\tau_B \leqslant 5$ μs. As this was already below the temporal resolution of our boxcar system, we were unable to measure its temperature dependence. In contrast, component A exhibits a dramatic variation, changing by three orders of magnitude between τ_A = 18.6 ms at 1.8 K and τ_A = 40 μs at 20 K. The overall temperature dependence is plotted in figure 8, together with the intensity ratio I_B/I_A after the necessary data correction has been performed. As can be seen from the figure, at low temperatures this ratio remains constant, decreasing linearly to zero for 8 K $\leqslant T \leqslant$ 13 K as the faster component B vanishes.

To simultaneously account for the measured temperature dependence of τ_A and the ratio I_B/I_A we tested several exciton models and found that a splitting in three substates A_1, A_2 and B is necessary (figure 9). A_1 and A_2 have to be in thermal equilibrium with each other, implying that the thermal transition probabilities are large compared to the radiative ones (W_{12}, $W_{21} \gg \Gamma_1, \Gamma_2$ in figure 9, left). Considering the limit W_{12}, $W_{21} \to \infty$, the analysis in terms of rate equations shows (Samiec 1990) that in this situation the time decay of states A_1 and A_2 is characterized by a single (effective) lifetime

$$\tau_{A,\mathrm{eff}} = \frac{1}{\Gamma_A^{\mathrm{eff}}} = \frac{g_1 + g_2 \exp(-(E_{A_2} - E_{A_1})/kT)}{g_1\Gamma_1 + g_2\Gamma_2 \exp(-(E_{A_2} - E_{A_1})/kT)}. \tag{5}$$

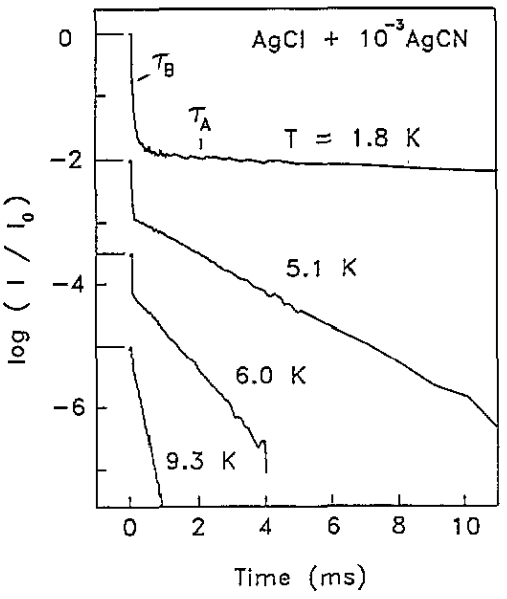

Figure 7. Time behaviour of the CN^- bound exciton luminescence intensity in AgCl + 10^{-3} AgCN at different temperatures. The non-exponential contribution to the decay is subtracted. The intensities are normalized to $I(t = 0)$; the curves are shifted along the ordinate for clearer representation. Laser excitation at 3.4 eV, detection at $E_D = 2.00\ eV$.

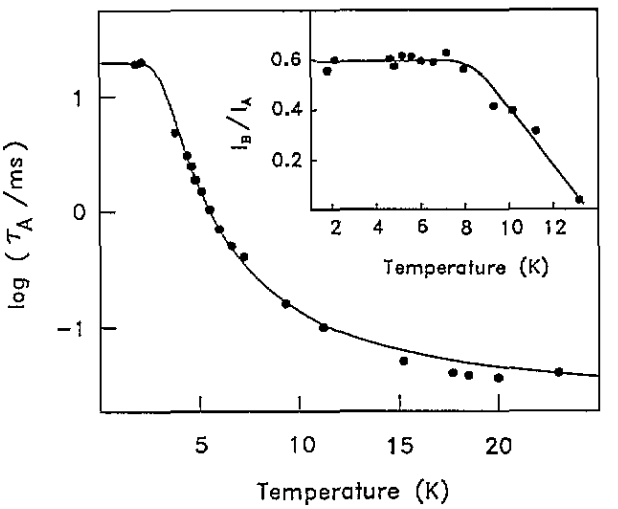

Figure 8. Temperature dependence of the effective time constant τ_A of the CN^- induced luminescence component A in logarithmic scale. The full curve through the data for τ_A is a fit according to equation (5). Inset: intensity ratio I_B/I_A of components A and B at different temperatures. The full line is a guide line for the eyes.

E_1, E_2 and g_1, g_2 designate the energies and degeneracies of the two states, the temperature dependence of $\tau_{A,eff}$ being due to thermal redistribution among them. We have used equation (5) to fit the experimental lifetime data and found excellent agreement (full curve in figure 8), choosing the following parameters:

$$\Delta E_{A_1A_2} = E_{A_1} - E_{A_2} = 2.1\ \text{meV} \qquad \tau_{A_1} = 1/\Gamma_{A_1} = 18.6\ \text{ms}$$

$$(g_2/g_1 = 3) \qquad (\tau_{A_2} = 1/\Gamma_{A_2} \leqslant 5\ \mu\text{s}).$$

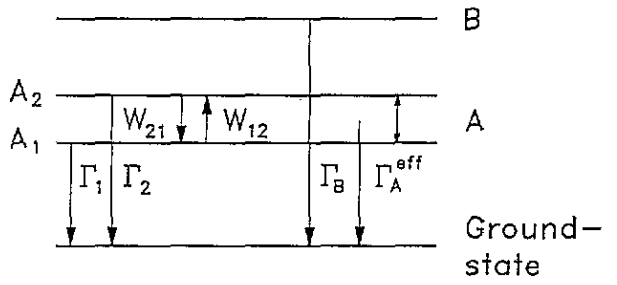

Figure 9. Energy level system for the CN^- bound exciton used to describe the experimental data. For nomenclature and explanations see text.

While for $E_{A_1A_2}$ and τ_{A_1} reliable values could be obtained from the fit, the quantities in parentheses turned out to be dependent on each other, so that one of them has to be fixed. Consistent with the proposed triplet and singlet character of the states (see below) we have chosen $g_2/g_1 = 3$.

As the energy splitting $\Delta E_{A_1A_2}$ is very much smaller than the width of each transition, the total emitted intensity at any detection photon energy E_D is approximately given by

$$I_A(t) \sim \Gamma_{A_1} n_{A_1}(t) + \Gamma_{A_2} n_{A_2}(t) = (n_{A_1}(0) + n_{A_2}(0))\Gamma_A^{eff} \exp(-\Gamma_A^{eff} t)$$
$$= A_0 \exp(-\Gamma_A^{eff} t) \tag{6}$$

where A_0 is a constant initial amplitude at $t = 0$ and n_{A_1}, n_{A_2} denote the time-dependent population numbers of exciton states A_1, A_2, respectively. The temporal behaviour found for the CN^- BX A component is completely consistent with equations (5) and (6), whereas state B, being characterized by a different time constant (τ_B), is clearly thermally decoupled from A.

With this in mind we consider the intensity ratio I_B/I_A (figure 8, inset). During the relaxation process that follows excitation, states A and B become occupied by corresponding rates R_A and R_B that comprise capture cross sections and the probabilities for the transition between the unrelaxed and relaxed states. By introducing corresponding decay rates Γ_A^{eff} and Γ_B (figure 9, right) and solving the rate equation system for the stationary case, it is straightforward to derive the relation

$$I_B/I_A = R_B/R_A. \tag{7}$$

Since experimentally this intensity ratio remains constant up to about 8 K (cf figure 8, inset), it is reasonable to assume that the relaxation rates into states A and B are temperature independent in this range. At higher temperatures, R_B/R_A obviously decreases because the rate R_B decreases and the rate R_A increases. Because both the total luminescence intensity and that of each component due to different defect centres are experimentally found to remain constant up to about 20 K (see figure 5), state A must be occupied at the expense of state B. All this implies that states A and B have a common unrelaxed excited state with the branching taking place during the final lattice relaxation.

3. Comparison with other isoelectronic impurities in AgCl

At this point a comparison between excitons bound to CN^- and other previously investigated isoelectronic impurities like Br^- and I^- in AgCl is appropriate. For this purpose we have

included in table 1 corresponding energy data for these impurity ions derived from the linear exciton–phonon coupling scheme illustrated in figure 4 (von der Osten and Stolz 1990). Applying the model approved to describe isoelectronic impurities in semiconductors (Dean and Herbert 1979), we regard the impurity ion as the responsible binding centre and the exciton to be centred at the defect lattice site. Then the difference in electron affinities of the substitutional host ion (here Cl^-) and the impurity ion represents a rough measure for the electronic potential provided by the defect to trap the hole part of the free exciton. Because CN^- doping leads to a BX in AgCl but not in AgBr (cf §2.1) it has to be assumed that the electron affinity $E_a(CN^-)$ lies in the range

$$3.61 \text{ eV} = E_a(Cl^-) > E_a(CN^-) \geqslant E_a(Br^-) = 3.36 \text{ eV}$$

which, referred to $E_a(Cl^-)$, corresponds to difference values between

$$0 \text{ eV} < \Delta E_a(CN^-) \leqslant 0.25 \text{ eV}.$$

Although ΔE_a is positive for all impurity ions considered here, inspection of table 1 shows that only in the case of AgCl:I^- is the electronic potential strong enough to cause a bound state ($E_0 - E_{gx}^i < 0$). In contrast, for CN^- and Br^- the energy difference $E_0 - E_{gx}^i > 0$, implying that the unrelaxed state at energy E_0 is degenerate with the FE band states. In these latter cases lattice relaxation is necessary to additionally stabilize the state and bring its energy below E_{gx}^i, as is actually observed.

Qualitatively this can be understood by considering the exciton binding mechanism in more detail. While the hole is localized at the defect ion and, to a first approximation, is built up by the uppermost electronic (p-like) wavefunctions of the isoelectronic impurity, the associated electron occupies the Ag^+ 5s states derived from the conduction band minimum. To account for the electron–lattice coupling the effect of the valence band states originating from the surrounding Ag^+ ions (d-like wavefunctions) and the Cl^- ions (p-like wavefunctions) has to be included in the consideration. In general, mixing the defect wavefunctions with those of the valence band causes a weakening of the defect potential, resulting in a delocalization of the hole. This effect, however, might be cancelled or even reversed if the defect potential is enhanced by lattice relaxation. In silver halides it is conceivable that lattice relaxation is caused by the high deformability of the Ag^+ ions surrounding the defect (Fischer 1974, Bilz and Weber 1984). The necessary coupling between the hole and the Ag^+ ions is mediated by the Ag^+ d wavefunctions, whereby the strength of the coupling is determined by their total contribution to the overall hole wavefunction.

Correspondingly, the relatively strong electronic potential in case of I^- will essentially concentrate the hole at the impurity with only small contributions of d functions from adjacent Ag^+ ions and, hence, weak electron–lattice relaxation. In contrast, due to the much weaker potential provided by the Br^- and CN^- impurities, the hole wavefunction in these cases is spread out, causing a high probability density at the Ag^+ ions and appreciable lattice coupling. Consistent with this we find the magnitude in lattice relaxation energy E_{LR} inversely correlated with the electronic energies (ΔE_a and $E_0 - E_{gx}^i$, respectively) of the respective defect, as seen in table 1.

For further discussion, table 2 shows splittings and lifetimes of the energy states observed for different impurity bound excitons. As described previously (§2), the CN^- BX is split into three substates (energies E_{A_1}, E_{A_2}, E_B) while a splitting into only two states (E_1, E_2) is found in case of Br^- and I^- with lifetimes as listed in the table. Having the same symmetry

as the replaced host ion, for atomic-type Br^- and I^- impurities a symmetry reduction caused by a local lattice distortion is likely to be responsible for the splitting of the originally eight-fold exciton state (Ahrenkiel 1968, von der Osten and Stolz 1990). For the CN^- ion, on the other hand, due to the molecular character of the impurity the symmetry is lower than that of the defect lattice site. Accordingly, the symmetry of the exciton must be adapted to the symmetry of the σ and π states of the CN^- molecular ion. As far as the orbital momentum wavefunction is concerned, this can result in a splitting of the exciton hole state into two or three substates depending on the so far unknown orientation of the CN^- molecular axis.

Table 2. Energy states and lifetimes observed for excitons bound to isoelectronic impurities in AgCl. Arrows indicate thermal equilibrium between states (see text). a, this work; b, Ahrenkiel (1968).

Impurity	Exciton states	Lifetimes	References
CN^-	E_B	$\tau_B \leqslant 5\ \mu s$	
	$E_{A_2} \longleftrightarrow E_{A_1}$	$\tau_{A_2} \leqslant 5\ \mu s$	a
	$\Delta E_{A_1A_2} = 2.1$ meV	$\tau_{A_1} = 18.6$ ms	
Br^-	E_1	$\tau_1 \leqslant 5\ \mu s$	
	E_2	$\tau_2 \sim 150\ \mu s$	a
I^-	$E_1 \longleftrightarrow E_2$	$\tau_1 = 3.1\ \mu s$	b
	$\Delta E_{12} = 0.73$ meV	$\tau_2 = 10.2\ \mu s$	

The spin character of the states is determined by the strength of the spin–orbit coupling and thus depends on the atomic number of the impurity ion. *LS* coupling for the hole and electron momenta, appropriate for CN^- (atomic number 13) would result in BX substates with nearly pure singlet and triplet character, respectively. It therefore seems reasonable to ascribe the short- and long-lived luminescence components observed for the CN^- BX to transitions from these states into the ground state. Different from this, the luminescence associated with the Br^- and I^- impurities (atomic numbers 35 and 53, respectively) originates from the well-known dipole-allowed A and forbidden B excitons (*jj*-coupled hole and electron) entirely analogous to the case of AgBr:I^- (Czaja and Baldereschi 1979). Here the substates have mixed spin character making it difficult to attribute the observed lifetimes without further experimental information.

4. Concluding remarks

In comparing the effect of isoelectronic CN^-, Br^- and I^- impurities on the exciton spectrum, we considered the defect as the binding centre to trap the hole which then is able to bind an electron to form the BX. As demonstrated above, the properties of the BX are closely related to those of the impurity, making it possible to describe the effect of all these impurities in a uniform picture with the hole of the BX extending more or less towards the adjacent Ag^+ ions.

While no further knowledge on the exciton structure can be obtained from optical spectroscopy alone, it is important to note that this model is different from that encountered in the context of the interpretation of optically detected magnetic resonance (ODMR) spectra for the Br^- associated exciton in AgCl (Hayes *et al* 1977, Marchetti and Tinti 1981, Yoshioka *et al* 1985, Spoonhower *et al* 1990). Here the hole is assumed to be centred at the Ag^+ ion, forming Ag^{2+} as in the case of the self-trapped exciton, whereby the

Br^- ion replaces one of the six Cl^- ions in the first shell around the silver ('STE(Br^-)'). Both models assume that the hole is simultaneously spread out over the impurity and the neighbouring Ag^+ ions, so that they can be considered as borderline cases of the same picture differing, however, in symmetry and dynamical properties.

As the CN^- BX luminescence, in comparison with the Br^- associated emission, is much more Stokes shifted and does not overlap with any intrinsic band, it appears to be a favourite candidate for further investigations, in particular by means of ODMR, to reveal the symmetry properties.

Acknowledgments

The authors appreciate support of the project by the Deutsche Forschungsgemeinschaft.

References

Ahrenkiel R K 1968 *Solid State Commun.* **6** 741

Bilz H and Weber W 1984 *The Physics of Latent Image Formation in Silver Halides* ed A Baldereschi, W Czaja, E Tosatti, M Tosi (Singapore: World Scientific) p 25

Burberry M S and Marchetti A P 1985 *Phys. Rev.* B **32** 1192

Czaja W and Baldereschi A 1979 *J. Phys. C: Solid State Phys.* **12** 405

Dean P J and Herbert D C 1979 *Excitons* (Springer Topics in Current Physics vol 14) ed K Cho (Berlin: Springer) p 55

Fischer K 1974 *Phys. Status Solidi* b **66** 295

Fitchen D B 1968 *Physics of Color Centres* ed W B Fowler (New York: Academic) p 294

Griffing K M and Simons J 1976 *J. Chem. Phys.* **64** 3610

Hayes W, Owen I B and Walker P J 1977 *J. Phys. C: Solid State Phys.* **10** 1751

Hotop H and Lineberger W C 1975 *J. Phys. Chem. Ref. Data* **4** 539

Joesten B L and Brown F C 1966 *Phys. Rev.* **148** 919

Kanzaki H 1986 *Excitonic Processes in Solids* (Springer Series in Solid State Sciences vol 60) ed M Cardona, P Fulde, K von Klitzing and H J Queisser (Berlin: Springer) p 309

Marchetti A P and Tinti D S 1981 *Phys. Rev.* B **24** 7361

Samiec D 1990 *Diplomarbeit* Universität Paderborn

Schulz M and von der Osten W 1993 *Phys. Status Solidi* b **177** 201

Shriver D F and Posner J 1966 *J. Am. Chem. Soc.* **88** 1672

Spoonhower J P, Ahlers F J, Eachus R S and McDougle W G 1990 *J. Phys.: Condens. Matter* **2** 3021

Stolz H, Schulz M and von der Osten W 1984 *The Physics of Latent Image Formation in Silver Halides* ed A Baldereschi, W Czaja, E Tosatti and M Tosi (Singapore: World Scientific) p 49

Toyozawa Y 1986 *Excitonic Processes in Solids* (Springer Series in Solid State Sciences vol 60) ed M Cardona, P Fulde, K von Klitzing and H J Queisser (Berlin: Springer) p 203

von der Osten W 1982 *I–VII Compounds, Landolt-Börnstein Numerical Data and Functional Relationships in Science and Technology, New Series III 17b: Semiconductors* ed O Madelung (Berlin: Springer) p 253

—— 1984 *Polarons and Excitons in Polar Semiconductors and Ionic Crystals* NATO ASI Series, series B: Physics **108** ed J T Devreese and F Peeters (New York: Plenum) p 293

von der Osten W and Stolz H 1990 *J. Phys. Chem. Solids* **51** 765

Yoshioka H, Sugimoto N and Yamaga M 1985 *J. Phys. Soc. Japan* **54** 3900